Investigating Near-fault Ground Motions with Dense Arrays

Report for SCEC Award #25250

Investigators and contributors: Xiaofeng Meng[1], Camilo Pinilla-Ramos[1,2], Yehuda Ben-Zion[1,3]

[1] SCEC
[2] GFZ
[3] USC

I. Project Overview

A. Abstract

In the box below, describe the project objectives, methodology, and results obtained and their significance. If this work is a continuation of a multi-year SCEC-funded project, please include major research findings for all previous years in the abstract. (Maximum 250 words.)

Following the Mw7.1 Ridgecrest, CA, earthquake, 15 dense 1D and 2D arrays (461 sites) were deployed around the main ruptures, including four 1D arrays across the surface rupture of the mainshock. The dense arrays captured numerous aftershocks with magnitudes in the range 0-5.2 within 10 km, and provided an unprecedented dataset for studying near-fault ground motions, which are crucial for near-fault hazards as they impose the strongest shaking and possible permanent displacements. However, In the current ground motion models (GMM), the near-fault motions are extrapolated from data recorded at moderate and large distances, assuming linear behavior which is not necessarily correct. Here, we combine the near-fault ground motion dataset from the Ridgecrest area with a regional dataset to develop a non-ergodic GMM. The developed GMM is used to investigate several aspects of the near-fault ground motions involving source, site, and path effects. Our initial findings include: 1) weak high-frequency energy radiation for shallow events; 2) significant variations in site responses within and around the fault zone in both fault-normal and fault-parallel directions; 3) strong frequency-dependent amplifications of ground motions within the fault zone. We propose to further analyze our near-fault GMM to constrain the effects of the damage zone, compare path effects between small and large events, investigate the near-fault saturation of ground motion, and compare our GMM to the regional GMMs.

B. SCEC Annual Science Highlights

Each year, the Science Planning Committee reviews and summarizes SCEC research accomplishments, and presents the results to the SCEC community and funding agencies. Rank (in order of preference) the sections in which you would like your project results to appear. Choose up to 3 working groups from below and re-order them according to your preference ranking.

1. Ground Motions
2. Seismology

C. Exemplary Figure

Select one figure from your project report that best exemplifies the significance of the results. The figure may be used in the SCEC Annual Science Highlights and chosen for the cover of the Annual Meeting Proceedings Volume. In the box below, enter the figure number from the project report, figure caption and figure credits.

Figure 2. (a) δS2S (red lines) and δWS (blue lines) from EAS versus distance to fault strike for arrays B1-B4 at 0.05s. The gray dashed line denotes the approximate location where the array intersects the surface ruptures. The horizontal green and red bars denote the low velocity zone and its inner core identified by Qiu et al., (2021), respectively. (b-e) Same figures with panel (a) at 0.1 s, 0.2 s, 0.5 s, and 1

s period, respectively. (f) The VS30 values along arrays B1-B4. (g1-g4) The cross-section of VP/VS from the 3D velocity model beneath arrays B1-B4.

D. SCEC Science Priorities

In the box below, please list (in rank order) the SCEC priorities this project has achieved. See *https://www.scec.org/research/priorities* for list of SCEC research priorities. *For example: 6a, 6b, 6c*

D3-3, B2-1

E. Intellectual Merit

How does the project contribute to the overall intellectual merit of SCEC? *For example: How does the research contribute to advancing knowledge and understanding in the field and, more specifically, SCEC research objectives? To what extent has the activity developed creative and original concepts?*

Near-fault ground motions produce the most severe seismic hazards, due to the strongest shaking, significant displacement, and pulse-like accelerations. However, in the current ground motion models (GMM), the lack of near-fault data, especially from large earthquakes, is a serious shortcoming. In GMMs, the near-fault ground motions are often extrapolated from the data recorded at moderate and large distances assuming linear behavior. Here we seek to systematically study the near-fault ground motions around the Ridgecrest mainshock rupture zone, by developing a partially non-ergodic near-fault GMM. The developed GMM decomposes the ground motion variations into the repeatable source, site, and path effects.

F. Broader Impacts

How does the project contribute to the broader impacts of SCEC as a whole? *For example: How well has the activity promoted or supported teaching, training, and learning at your institution or across SCEC? If your project included a SCEC intern, what was his/her contribution? How has your project broadened the participation of underrepresented groups? To what extent has the project enhanced the infrastructure for research and education (e.g., facilities, instrumentation, networks, and partnerships)? What are some possible benefits of the activity to society?*

We develop a near-fault non-ergodic GMM based on small earthquakes and dense arrays data, which shed light on several scientific and engineering problems related to earthquake physics, fault zone properties, and seismic hazard. In particular, our study indicates that the variability in near-fault ground motions cannot be extrapolated from global GMMs and underscores the importance of exercising caution when modeling ground motion near active fault zones, where the spatial correlation is very short. Local non-ergodic GMMs are crucial for improving both the median predictions and uncertainty in near-fault ground motion modeling.

G. Project Publications

All publications and presentations of the work funded must be entered in the SCEC Publications database. Log in at *http://www.scec.org/user/login* and select the Publications button to enter the SCEC Publications System. Please either (a) update a publication record you previously submitted or (b) add new publication record(s) as needed. If you have any problems, please email *web@scec.org* for assistance.

SCEC Contribution #15027

Meng, X., Pinilla-Ramos, C., Kottke, A., & Ben-Zion, Y. (2025). Investigating Near-Fault Ground Motions Using Data Recorded by Dense Arrays Around the 2019 Mw 7.1 Ridgecrest, California, Earthquake

Rupture. *Bulletin of the Seismological Society of America*, 115(6), 2721-2740. https://doi.org/10.1785/0120250092.

II. Technical Report

The technical report should describe the project objectives, methodology, and results obtained and their significance. If this work is a continuation of a multi-year SCEC-funded project, please include major research findings for all previous years in the report. (Maximum 5 pages, 1-3 figures with captions, references and publications do not count against the limit.)

Investigating Near-fault Ground Motions with Dense Arrays

Report for SCEC Award #25250

Investigators and contributors: Xiaofeng Meng, Camilo Pinilla-Ramos, Yehuda Ben-Zion

1. Introduction

One major obstacle to progress in earthquake research is the lack of near-fault recordings (<10 km), particularly from large earthquakes. Reliable quantifications of the near-fault ground motions are crucial for site-specific probabilistic seismic hazard analysis (PSHA) for critical infrastructures near or cross fault zones, such as power plants, bridges, pipelines, high-rise buildings, dams and so forth. Near-fault ground motions impose the most severe seismic hazards, due to the strongest shaking, possible significant displacement (e.g., Goulet et al. 2021), and pulse-like accelerations (e.g., Alavi and Krawinkler 2004). However, in the current ground motion models (GMM), the lack of the near-fault data, especially from large earthquakes, is a glaring shortcoming (e.g., Ancheta et al. 2014; Bozorgnia et al. 2014). In GMMs, the near-fault ground motions are often extrapolated from the data recorded at moderate and large distances assuming linear behavior (e.g., Abrahamson et al. 2014), which may not necessarily be correct due to near-source saturation and anelastic attenuation.

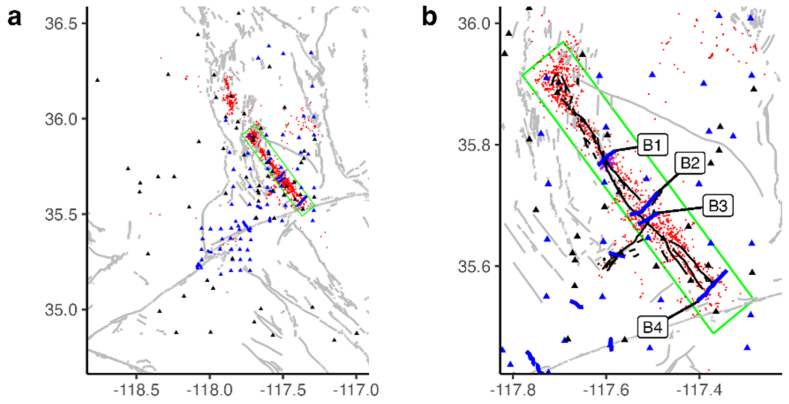

Figure 1. (a) Map of the study area around Ridgecrest, CA. Red dots denote aftershocks of the M_w7.1 Ridgecrest earthquake. Black triangles denote the permanent seismic stations. Blue triangles denote the temporary dense arrays. The green box denotes the fault zone of the M_w7.1 Ridgecrest earthquake. Gray lines denote the other faults. (b) Zoom-in map of the fault zone. Gray lines denote the surface ruptures of the M_w6.4 and M_w7.1 Ridgecrest earthquakes. Blue lines and triangles denote the temporary node arrays.

On 4 July 2019, a M_w6.4 earthquake ruptured a NE–SW-trending fault near Ridgecrest, California. Approximately 34 hours later, another M_w7.1 earthquake (hereafter the mainshock) occurred on an orthogonal NW–SE-trending fault close to the epicenter of the M_w6.4 event (Brandenberg et al. 2020). Starting at ~one day following the M_w7.1 mainshock, 461 three-component nodal seismometers (nodes) were deployed around the main ruptures in 15 1D or 2D dense arrays (Figure 1a) and continuously recorded for ~two months (Catchings et al. 2020). The dense arrays recorded numerous aftershocks between magnitude 0 and 5.2, the majority of which have hypocentral distances smaller than 20 km. Among the 15 arrays, four 1D arrays (B1-B4) were deployed across the surface ruptures of the mainshock (Figure 1b), with ~100 m spacing and apertures of 4 to 8 km. The numbers of nodes in arrays B1, B2, B3, and B4 are 46, 72, 46, and 84, respectively. The large number of recordings within close proximity of the Ridgecrest fault

zone makes it an unprecedented dataset for studying near-fault ground motions and fault structures.

2. Data

The earthquake catalog we use is the relocated catalog by Hauksson et al. (2012), which is extended to the current date. We only keep events with M_L>2 and R_{hyp}<100 km, as they are less affected by overlapping microearthquakes. As a result, we end up with 9207 aftershocks recorded by the nodal arrays. The Pseudo Spectral Acceleration (PSA) RotD50, which represents the median value of the maximum acceleration from all nonredundant rotations of the two horizontal components, and Effective Amplitude Spectra (EAS) from each recording are computed with the predicted durations at various periods. Rekoske et al. (2020) developed a regional ground motion dataset for the Ridgecrest sequence using permanent seismometers. The regional dataset contains 22,375 records from 131 events of M 3.6-7.1 at 968 sites. To improve the distance and azimuth coverage and stabilize the magnitude scaling in regression, we combine the ground motions from the nodal arrays with the regional Ridgecrest ground motion dataset. We only retain recordings from the regional dataset that are within 100 km of the hypocenters . As a result, 2806 recordings from 113 events and 71 sites from the regional dataset are combined with the nodal array dataset. Our final ground motion dataset contains ~800,000 recordings.

3. Ground Motion Model

We first perform the mixed-effects regression (Abrahamson and Youngs 1992) on the combined ground motion dataset with the following functional form to obtain an ergodic GMM:

$$\ln(Y) = b_1 + b_2 M + b_3 M^2 + (b_4 + b_5 M)\ln\left(\sqrt{R_{hyp}^2 + h^2}\right) + b_6 \ln\left(\frac{V_{S30}}{500}\right) + b_7 R_{hyp} + b_8 Z_{hyp} + b_9 F_n + b_{10} F_{rv} + b_{11} f(Z_{2.5}) + \delta B_e + \delta W_{es} \quad (1)$$

where M is local magnitude; Z_{hyp} is the hypocentral depth; F_n and F_{rv} are indicators for normal and reverse faulting mechanisms, and the other terms were defined earlier. The effective depth term h is defined following Abramason et al. (2014):

$$h = \begin{cases} 1 & M \leqslant 4 \\ 4.5 - 3.5 \times (5 - M) & 4 < M < 5 \\ 4.5 & M \geqslant 5 \end{cases} \quad (2)$$

The basin response term f($Z_{2.5}$) is referenced from Campbell and Bozorgnia (2014):

$$f(Z_{2.5}) = \begin{cases} b_{11}(Z_{2.5} - 1) & Z_{2.5} \leqslant 1 \\ 0 & 1 < Z_{2.5} < 3 \\ b_{12} e^{-0.75}\left[1 - \left(\exp\left(-0.25\left(Z_{2.5} - 3\right)\right)\right)\right] & Z_{2.5} \geqslant 3 \end{cases} \quad (3)$$

At this stage, the only random effect included in regression is the event id e. δB_e and δW_{es} is the between-event and within-event residual, respectively. After removing the systematic patterns identified at the event level, we develop a partially non-ergodic GMM, in which the within-event residuals are decomposed into two components:

$$\delta W_{es} = \delta S2S_s + \delta WS_{es} \quad (4)$$

where $\delta S2S_s$ is the site term, which represents the site responses at site ‘s’ that are not captured by V_{S30} and $Z_{2.5}$ scaling in the ergodic GMM (i.e., the systematic statistical difference or pattern a site develops with respect to the ergodic model). Because the majority of events are located within the fault zone of the Ridgecrest mainshock, at sites that are within or close to the fault zone, wave propagation effects within the fault zone (e.g., scattering, trapped waves, etc.) would

be mapped into δS2S, which prevent us from examining the genuine near-fault site responses. Therefore, δS2S is estimated using residuals from events outside the fault zone only (i.e. events outside the green box in Figure 1). δWS_{es} is the within-site residual, which contains all the unmodeled effects that depend on both event's and site's location, including wave propagation, radiation pattern, directivity, and aleatory variations.

4. Results

4.1. Ground motion amplifications within the fault zone

A damage zone within the fault zone, which has significantly lower seismic velocities compared to the hosting rocks on either side of the fault, could amplify ground motions(Cormier and Spudich 1984; Lewis and Ben-Zion 2010; Igel et al. 2002). The amplifications are caused by the combination of reduced seismic velocities and wave interference within the damage zone. In recent years, several studies have conducted detailed investigations of the ground motions

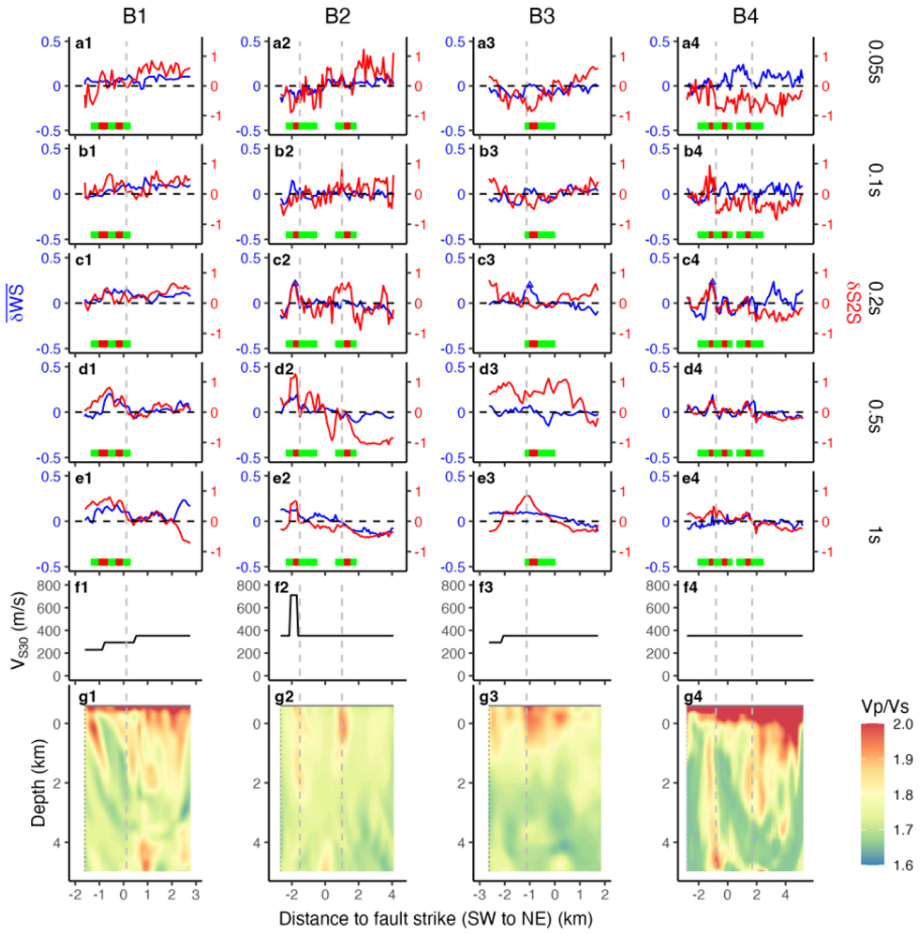

Figure 2. (a) *δS2S* (red lines) and *δWS* (blue lines) from EAS versus distance to fault strike for arrays B1-B4 at 0.05s. The horizontal green and red bars denote the low velocity zone and its inner core identified by Qiu et al., (2021), respectively. (b-e) Same figures with panel (a) at 0.1 s, 0.2 s, 0.5 s, and 1 s period, respectively. (f) The V_{S30} values along arrays B1-B4. (g1-g4) The cross-section of V_p/V_s from the 3D velocity model beneath arrays B1-B4.

amplifications across fault zones using dense arrays.

In Figure 2a-2e, the red curves represent S2S from the partially non-ergodic GMM along arrays B1-B4 at 0.05 s, 0.1 s, 0.2 s, 0.5 s and 1 s, along with V_{S30} values (Figure 2f) and the 3D velocity model underneath each array (Figure 2g). The main damage zones underneath arrays B2

and B4 can be clearly identified by the combination of surface ruptures (vertical gray dashed lines in Figure 2) and a narrow vertical zone of high V_P/V_S anomalies from the 3D velocity model. Moreover, Qiu et al., (2021) identified the low velocity zones (green bars in Figure 2) and the more intensely damaged inner core (red bars in Figure 2) by analyzing delay times between P-waves from ~1200 local earthquakes and four teleseismic events at arrays B1-B4. For arrays B1, B2 and B4, we observe elevated δS2S within the main damage zones at selected periods (0.5 s and 1 s for B1; 0.2 s, 0.5 s, and 1 s for B2; 0.1 s, 0.2 s, and 0.5 s for B4). The few-hundred-meter spatial extensions of sites with elevated δS2S at arrays B1, B2, and B4 are consistent with the inner cores, as well as the widths of the high V_P/V_S anomalies from the 3D velocity model, which is the typical width of a fault damage zone(Vidale and Li 2003; Li et al. 2004; Ben-Zion et al. 2003a; Peng et al. 2003). In the Ridgecrest area, Qiu et al.(2021) inverted trapped waves from 33 events and six nodes in array B4 for the fault zone structure. The best-fitting model yields a vertical rectangular-shaped damage zone with a width of ~280 m. Since V_{S30} values from the Thompson map do not capture the low velocity damage zone, the elevated δS2S are likely the results of the overestimated V_{S30} values at nodes within the damage zones.

Underneath array B3, no well-defined damage zone can be seen in the 3D velocity model. We also do not find increased δS2S around the surface ruptures at any period, except for array B3 at 1 s. For arrays B1-B4, there are also significant variations outside the damage zones, which do not correlate well with the 3D velocity model.

Similar to δS2S, there are significant variations of δWS within each array and between arrays (blue curves in Figure 2a-e), suggesting complicated wave propagation effects in the fault zone. A sufficiently coherent fault damage zone can act as a waveguide and generate trapped waves resulting from constructive interference of critically reflected waves within the waveguide(Li et al. 1990; Ben-Zion and Aki 1990; Qiu et al. 2020; Jahnke et al. 2002). At array B1, elevate near the inner core at 0.5 s and 1 s period. At arrays B2 and B4, clearly increase near the inner core between 0.1 s and 0.5 s period. At array B3, there are evident larger near the inner core between 0.05 s and 0.2 s period. The elevated support the existence of trapped waves within the Ridgecrest rupture zone, as was found by Qiu et al. (2021). The period range is also consistent with the dominant frequency of ~5 Hz found by previous studies on the fault zone trapped waves(Ben-Zion et al. 2003b; Peng et al. 2003; Qiu et al. 2017).

4.2. Radiation pattern effects

Because the radiation pattern effects are dependent on both event and site locations, they are included in WS_{es} in the partially non-ergodic GMM. Therefore, we explore the radiation pattern effects on ground motions by plotting δWS_{es} as a function of the azimuth measured from each event's strike to the epicenter-to-site direction (Figure 3). At longer periods (0.2-1 s), there are subtle but evident cosine-like signals for M<4 events, which are consistent with the radiation patterns of vertical strike-slip faulting that is dominant in our dataset. At 0.05 s and 0.1 s period, the radiation pattern signals disappear, and WS_{es} become approximately isotropic with fluctuations. For M 4-5 events, the lack of clear radiation patterns at any period is probably due to the small number of events. Since the attenuation has been ruled out in the analysis, the disappearance of radiation patterns at short periods support that the earthquake rupture process is period dependent. At long periods, the rupture process can be well described with a double-couple model. At short periods, significant non-double couple components due to source and fault zone complexity appear dominant. The candidate processes include CLVD due to the

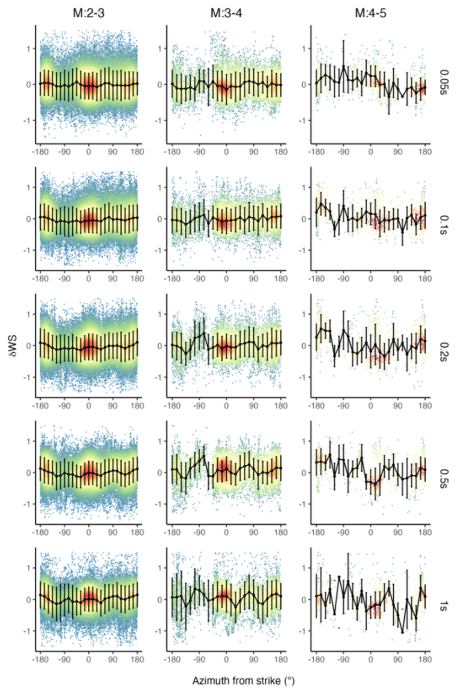

Figure 3. *δWS* from EAS versus azimuth from strike computed from different magnitude groups and at different periods, color-coded by the density. The lines and error bars denote the average values and one standard deviation.

activation of subsidiary smaller faults(e.g., Julian et al. 1998), wave scattering in the fault zone damage structure(e.g., Touma et al. 2022), slipping on non-planar surfaces(Castro et al. 1992; e.g., Lomnitz-Adler 1991), and isotropic radiation from rock damage generation(e.g., Ben‐Zion and Ampuero 2009). Capturing the period-dependent radiation patterns has crucial implications for improving seismic hazard analysis, as the empirical GMMs do not explicitly account for radiation pattern effects(Abrahamson et al. 2014; Campbell and Bozorgnia 2014; Boore et al. 2014; Chiou and Youngs 2014). The results from our study, along with a few others(Kotha et al. 2019; Huang et al. 2023), provide a basis for better understanding of radiation patterns' effects on ground motions and eventual inclusion of radiation pattern effects in future GMMs.

References

Abrahamson, N. A., and R. R. Youngs. 1992. "A Stable Algorithm for Regression Analyses Using the Random Effects Model." *Bulletin of the Seismological Society of America* 82 (1): 505–510.

Abrahamson, Norman A., Walter J. Silva, and Ronnie Kamai. 2014. "Summary of the ASK14 Ground-Motion Relation for Active Crustal Regions." *Earthquake Spectra* 30 (3): 1025–1055.

Alavi, Babak, and Helmut Krawinkler. 2004. "Behavior of Moment‐resisting Frame Structures Subjected to Near‐fault Ground Motions." *Earthquake Engineering & Structural Dynamics* 33 (6): 687–706.

Ancheta, Timothy D., Robert B. Darragh, Jonathan P. Stewart, et al. 2014. "NGA-West 2 Database." *Earthquake Spectra* 30 (3): 989–1005.

Ben‐Zion, Y., and J. Ampuero. 2009. "Seismic Radiation from Regions Sustaining Material Damage." *Geophysical Journal International* 178 (3): 1351–1356.

Ben-Zion, Yehuda, and Keiiti Aki. 1990. "Seismic Radiation from an*SH*line Source in a Laterally Heterogeneous Planar Fault Zone." *Bulletin of the Seismological Society of America* 80 (4): 971–994.

Ben-Zion, Yehuda, Zhigang Peng, David Okaya, et al. 2003a. "A Shallow Fault-Zone Structure Illuminated by Trapped Waves in the Karadere–Duzce Branch of the North Anatolian Fault, Western Turkey." *Geophysical Journal International* 152 (3): 699–717.

Ben-Zion, Yehuda, Zhigang Peng, David Okaya, et al. 2003b. "A Shallow Fault-Zone Structure Illuminated by Trapped Waves in the Karadere-Duzce Branch of the North Anatolian Fault, Western Turkey." In *Geophysical Journal International*, vol. 152, 152. no. 3. Preprint. https://doi.org/10.1046/j.1365-246x.2003.01870.x.

Boore, David M., Jonathan P. Stewart, Emel Seyhan, and Gail M. Atkinson. 2014. "NGA-West2 Equations for Predicting PGA, PGV, and 5% Damped PSA for Shallow Crustal Earthquakes." *Earthquake Spectra* 30 (3): 1057–1085.

Bozorgnia, Yousef, Norman A. Abrahamson, Linda Al Atik, et al. 2014. "NGA-West2 Research Project." *Earthquake Spectra* 30 (3): 973–987.

Brandenberg, Scott J., Jonathan P. Stewart, Pengfei Wang, et al. 2020. "Ground Deformation Data from GEER Investigations of Ridgecrest Earthquake Sequence." *Seismological Research Letters* 91 (4): 2024–2034.

Campbell, Kenneth W., and Yousef Bozorgnia. 2014. "NGA-West2 Ground Motion Model for the Average Horizontal Components of PGA, PGV, and 5%-Damped Linear Acceleration Response Spectra." *Earthquake Spectra* 30 (3): 1087–1115.

Castro, R. R., J. G. Anderson, and J. N. Brune. 1992. "P and S-Wave Displacements from Kinematic Dislocation Models." *Bulletin of the Seismological Society of America* 82 (4): 1910–1926.

Catchings, Rufus D., Mark R. Goldman, Jamison H. Steidl, et al. 2020. "Nodal Seismograph Recordings of the 2019 Ridgecrest Earthquake Sequence." *Seismological Research Letters* 91 (6): 3622–3633.

Chiou, Brian S-J, and Robert R. Youngs. 2014. "Update of the Chiou and Youngs NGA Model for the Average Horizontal Component of Peak Ground Motion and Response Spectra." In *Earthquake Spectra*, vol. 30, 30. no. 3. Preprint. https://doi.org/10.1193/072813eqs219m.

Cormier, V. F., and P. Spudich. 1984. "Amplification of Ground Motion and Waveform Complexity in Fault Zones: Examples from the San Andreas and Calaveras Faults." *Geophysical Journal International* 79 (1): 135–152.

Goulet, Christine A., Yongfei Wang, Chukwuebuka C. Nweke, et al. 2021. "Comparison of Near‐Fault Displacement Interpretations from Field and Aerial Data for the M 6.5 and 7.1 Ridgecrest Earthquake Sequence Ruptures." *Bulletin of the Seismological Society of America* 111 (5): 2317–2333.

Hauksson, E., W. Yang, and P. M. Shearer. 2012. “Waveform Relocated Earthquake Catalog for Southern California (1981 to June 2011).” *Bulletin of the Seismological Society of America* 102 (5): 2239–2244.

Huang, Jyun-Yan, Chih-Hsuan Sung, Shu-Hsien Chao, and Norman A. Abrahamson. 2023. “Including Radiation-Pattern Effects in Ground-Motion Models for Taiwan.” *Bulletin of the Seismological Society of America*, ahead of print, February 13. https://doi.org/10.1785/0120220167.

Igel, H., G. Jahnke, and Y. Ben-Zion. 2002. “Numerical Simulation of Fault Zone Guided Waves: Accuracy and 3-D Effects.” *Pure and Applied Geophysics* 159 (9): 2067–2083.

Jahnke, Gunnar, Heiner Igel, and Yehuda Ben-Zion. 2002. “Three-Dimensional Calculations of Fault-Zone-Guided Waves in Various Irregular Structures.” *Geophysical Journal International* 151 (2): 416–426.

Julian, Bruce R., Angus D. Miller, and G. R. Foulger. 1998. “Non‐double‐couple Earthquakes 1. Theory.” *Reviews of Geophysics (Washington, D.C.: 1985)* 36 (4): 525–549.

Kotha, Sreeram Reddy, Fabrice Cotton, and Dino Bindi. 2019. “Empirical Models of Shear-Wave Radiation Pattern Derived from Large Datasets of Ground-Shaking Observations.” *Scientific Reports* 9 (1): 981.

Lewis, Michael A., and Yehuda Ben-Zion. 2010. “Diversity of Fault Zone Damage and Trapping Structures in the Parkfield Section of the San Andreas Fault from Comprehensive Analysis of near Fault Seismograms.” *Geophysical Journal International* 183 (3): 1579–1595.

Li, Y. G., P. Leary, K. Aki, and P. Malin. 1990. “Seismic Trapped Modes in the Oroville and San Andreas Fault Zones.” *Science (New York, N.Y.)* 249 (4970): 763–766.

Li, Yong-Gang, John E. Vidale, and Elizabeth S. Cochran. 2004. “Low-Velocity Damaged Structure of the San Andreas Fault at Parkfield from Fault Zone Trapped Waves.” In *Geophysical Research Letters*, vol. 31, 31. no. 12. Preprint. https://doi.org/10.1029/2003gl019044.

Lomnitz-Adler, Jorge. 1991. “Model for Steady State Friction.” *Journal of Geophysical Research* 96 (B4): 6121–6131.

Peng, Zhigang, Yehuda Ben-Zion, Andrew J. Michael, and Lupei Zhu. 2003. “Quantitative Analysis of Seismic Fault Zone Waves in the Rupture Zone of the 1992 Landers, California, Earthquake: Evidence for a Shallow Trapping Structure.” *Geophysical Journal International* 155 (3): 1021–1041.

Qiu, H., Y. Ben-Zion, Z. E. Ross, P-E Share, and F. L. Vernon. 2017. “Internal Structure of the San Jacinto Fault Zone at Jackass Flat from Data Recorded by a Dense Linear Array.” *Geophysical Journal International* 209 (3): 1369–1388.

Qiu, Hongrui, Amir A. Allam, Fan-Chi Lin, and Yehuda Ben-Zion. 2020. “Analysis of Fault Zone Resonance Modes Recorded by a Dense Seismic Array across the San Jacinto Fault Zone at Blackburn Saddle.” *Journal of Geophysical Research. Solid Earth* 125 (10). https://doi.org/10.1029/2020jb019756.

Qiu, Hongrui, Yehuda Ben-Zion, Rufus Catchings, Mark R. Goldman, Amir A. Allam, and Jamison Steidl. 2021. “Seismic Imaging of the MW 7.1 Ridgecrest Earthquake Rupture Zone from Data Recorded by Dense Linear Arrays.” *Journal of Geophysical Research. Solid Earth* 126 (7). https://doi.org/10.1029/2021jb022043.

Rekoske, John M., Eric M. Thompson, Morgan P. Moschetti, Mike G. Hearne, Brad T. Aagaard, and Grace A. Parker. 2020. “The 2019 Ridgecrest, California, Earthquake Sequence Ground Motions: Processed Records and Derived Intensity Metrics.” *Seismological Research Letters* 91 (4): 2010–2023.

Touma, Rita, Alexandre Aubry, Yehuda Ben-Zion, and Michel Campillo. 2022. “Distribution of Seismic Scatterers in the San Jacinto Fault Zone, Southeast of Anza, California, Based on Passive Matrix Imaging.” *Earth and Planetary Science Letters* 578 (117304): 117304.

Vidale, John E., and Yong-Gang Li. 2003. “Damage to the Shallow Landers Fault from the Nearby Hector Mine

Earthquake.” *Nature* 421 (6922): 524–526.